PNAS RESEARCH ARTICLE | NEUROSCIENCE OPEN ACCESS

Dark continuous noise from visual pigment as a major mechanism underlying rod–cone difference in light sensitivity

Zuying Chai[a,1], Daniel Silverman[a,b,2,3], Sihan Li[a,4], Parinaz Bina[a,5], and King-Wai Yau[a,c,1]

Affiliations are included on p. 11.

Contributed by King-Wai Yau; received September 4, 2024; accepted November 7, 2024; reviewed by Ching-Kang J. Chen and Theodore G. Wensel

Retinal rods and cones underlie scotopic and photopic vision, respectively. Their pigments exhibit spontaneous isomerizations (quantal noise) in darkness due to intrinsic thermal energy. This quantal noise, albeit exceedingly low in rods, dictates the light threshold for scotopic vision. The same quantal noise in cones, however, is too low to explain the much higher diurnal light threshold. Separately, a dark continuous noise is present in rods, long accepted to originate from an intrinsic random activation of the cyclic guanosine monophosphate (cGMP)-phosphodiesterase enzyme mediating phototransduction downstream of the pigment. Here, we report the surprising finding that most of this rod dark continuous noise actually originates from rhodopsin itself. Importantly, we found the same continuous noise with a much higher magnitude from cone pigments. The rod and cone continuous noises are apparently both associated with a hitherto unrecognized "metastable" pigment conformational state physiologically resembling that in apo-opsin (opsin devoid of chromophore) and is intermittently active for very brief moments. The cone holopigment's high continuous noise is expected to act as an intrinsic equivalent light and adapt the cone dramatically, accounting for a major part of the light-sensitivity difference between rods and cones in darkness.

dark continuous noise | visual pigment | rods and cones | sensitivity

Significance

Retinal rods exhibit two kinds of dark spontaneous phototransduction activity. One is quantal noise originating from thermal isomerization of rhodopsin. The other is continuous noise believed for almost three decades to come from intrinsic activity of the phosphodiesterase enzyme mediating phototransduction. The rod quantal noise dictates the scotopic light threshold, but what limits the photopic light threshold remains unclear. We found here, surprisingly, that the rod dark continuous noise actually comes from rhodopsin, and we have just identified a similar dark continuous noise from cone pigments even far higher in magnitude. We expect this high cone-pigment continuous noise to produce native-cone adaptation constitutively and sufficiently in darkness to explain a major proportion of the absolute rod–cone difference in light sensitivity.

Our image-forming vision begins in retinal rods and cones with the absorption of photons by the visual pigments, which activate the downstream G-protein, transducin (G_{T1} for rod transducin and G_{T2} for cone transducin). Active transducin (G_{T1}* or G_{T2}*) in turn stimulates its effector enzyme, the cGMP-phosphodiesterase (PDE*) (comprising rod and cone isoforms) to hydrolyze cGMP. The lowered cGMP concentration leads to the closure of some cyclic-nucleotide-gated (CNG), nonselective cation channels open in darkness, producing a membrane hyperpolarization as the light response (1–3). This overall process, termed phototransduction, converts photon energy into a neural electrical signal that the retina and the brain can understand (1–3).

In darkness, rods and cones display spontaneous phototransduction activities called dark noise (4–12). One noise component is quantal noise, coming from spontaneous (thermal) isomerization of single visual-pigment molecules due to internal thermal energy and manifesting electrically as being identical in size and shape to the responses to single absorbed photons (7, 8, 13, 14). The rod quantal noise in some animal species, such as toad, is directly observable because their unitary events are large enough for resolution from background noise (7). In some other species, such as mouse, the single-photon responses in rods (and therefore also the individual spontaneous isomerization events) are somewhat smaller and often require amplification for detection via removal of a Ca^{2+}-mediated, negative-feedback control mechanism that regulates phototransduction (13, 15). In cones, the quantal noise is much too small for direct detection, but can be resolved by expressing a cone pigment heterologously in rods to allow the active cone pigment to signal through the higher-gain rod phototransduction mechanism (15, 16).

In addition, a second phototransduction noise component in darkness has been detected along with quantal noise, and named "continuous" noise. It comprises unitary events that are much smaller than thermal isomerizations but occur far more frequently, hence dubbed "continuous noise" (7). It was initially described only in rods, and characterized based on its kinetics to originate from somewhere in the middle of the phototransduction signaling cascade (7). For the past almost thirty years, it has become largely accepted that this continuous noise arises from random, intrinsic activation of the rod PDE enzyme molecules downstream from the photopigment and the G-protein in phototransduction (11, 17).

[1]To whom correspondence may be addressed. Email: zchai1@jhmi.edu or kwyau@jhmi.edu.

[2]Present address: HHMI, University of California Berkeley, Berkeley, CA 94720.

[3]Present address: Department of Neuroscience, Helen Wills Neuroscience Institute, University of California Berkeley, Berkeley, CA 94720.

[4]Present address: Department of Ophthalmology, Mount Sinai School of Medicine, New York City, NY 10029.

[5]Present address: School of Biological Sciences, University of California San Diego, La Jolla, CA 92093.

This article contains supporting information online at https://www.pnas.org/lookup/suppl/doi:10.1073/pnas.2418031121/-/DCSupplemental.

Published December 10, 2024.

The quantal noise in rods is quite uniform across vertebrate species, with a human cellular rate of ~1 event min^{-1} $cell^{-1}$ at 37 °C (7, 8), matching the threshold for nocturnal vision measured in human psychophysical experiments and mouse behavioral studies (18–22). In other words, extrinsic light has to override this background noise in order to be perceived. For cones, an early study on turtle showed that a dark noise exists that probably originates from random openings of the light-sensitive CNG channels (5). Two subsequent studies on salamander LW-cones ("LW" for long-wavelength-sensitive) reported that the dark noise was dominated by spontaneous isomerization (23, 24), whereas a third suggested the major noise source to be apo-opsin originating from a tendency of LW-pigment to dissociate spontaneously in darkness into free opsin and chromophore without isomerization (25). Another study on fish cones, nonetheless, again suggested that the dark noise came mostly from spontaneous PDE activity as in rods (26), whereas yet another attributed it again to cone apo-opsin from chromophore dissociation without isomerization (27). In other words, the situation for cones remains unclear, especially mammalian cones, where the dark noise has been reported to originate mostly from an unknown source instead of spontaneous cone-pigment isomerization (28–30).

In the present work, we unwittingly found that the holopigments, whether in rods or in cones, are actually the source of most of this continuous noise, originating from a previously unrecognized metastable conformational state of the pigment molecule intermittently activating transduction at a fairly high rate albeit of low amplitude. In cones, this continuous pigment noise is especially much higher than quantal noise, constitutively adapting the cone sufficiently in darkness to become the main factor underlying the large rod/cone difference in sensitivity.

Results

Dark Continuous Noise from Rhodopsin. Fig. 1 *A*, *Left* shows suction-pipette recording (31, 32) in darkness from a wild-type ($Rho^{WT/WT}$) mouse rod in a freshly isolated retinal slice at 37 °C, with a dark current close to 15 pA measured with a saturating flash (Fig. 1 *A*, *Middle*; collective data shown in Fig. 1*D*). In darkness, the discrete events (marked by stars in all of the figures) indicative of spontaneous isomerization of rhodopsin were barely resolvable. The continuous noise in the background was also hardly distinguishable from instrumental noise measured in saturating light (Fig. 1 *A*, *Right*). To improve signal resolution, we adopted the $Gcaps^{-/-}$ background, in which rod sensitivity was increased by ~fivefold by removal of a Ca^{2+}-mediated negative feedback (33–35). As expected, the spontaneous-isomerization events in the $Gcaps^{-/-}$ background increased dramatically in amplitude, revealing a cellular rate of ~1 event min^{-1} (Fig. 1 *B*, *Left*, mean ± SD = 0.52 ± 0.26 event min^{-1}). The continuous noise also became sufficiently prominent to be distinct from the instrumental noise (Fig. 1 *B*, *Left* and *Right*); its variance increased from σ^2 = 0.046 ± 0.011 pA^2 for $Rho^{WT/WT}$ to σ^2 = 0.162 ± 0.077 pA^2 for $Rho^{WT/WT};Gcaps^{-/-}$, with the dark current largely unchanged (Fig. 1 *B*, *D*, and *E*). We happened to have recorded from another mouse line in the $Gcaps^{-/-}$ background in which rhodopsin (WT-Rho) was replaced by the "largely functionally silenced" mutant, REY-Rho ($Rho^{REY/REY};Gcaps^{-/-}$ line; 35). The REY-Rho mutant severely impairs rhodopsin's binding to the rod G-protein, transducin ($G_{T1}\alpha$ or *Gnat1*), rendering its associated single-photon response (and also the spontaneous-isomerization events) far too small to be visible (Fig. 1 *C*, *Left*). Overall, $Rho^{REY/REY};Gcaps^{-/-}$rods are 7,400-fold less sensitive than $Rho^{WT/WT};Gcaps^{-/-}$. However, the expression level of REY-Rho and its light absorption remain normal, as are the outer-segment structure and the expression level of other phototransduction proteins (35, 36). The surprise is that, despite a normal dark current (Fig. 1 *C*, *Middle*), the dark continuous noise in $Rho^{REY/REY};Gcaps^{-/-}$ rods became much lower, with σ^2 = 0.066 ± 0.024 pA^2 (Fig. 1 *C*, *Left*; statistics in Fig. 1*E*). Thus, the continuous noise in WT mouse rods appears to come mostly from rhodopsin instead of the intrinsic activation of PDE, which is downstream of rhodopsin in phototransduction and therefore should not be affected by REY-Rho replacing WT-Rho. In addition, exogenous 11-*cis*-retinal, the chromophore that binds covalently to apo-opsin via a Schiff base to form holo-pigment, did not change the continuous noise of $Rho^{WT/WT};Gcaps^{-/-}$ rods (*SI Appendix*, Fig. S1; see also ref. 35), excluding apo-opsin's presence in WT-Rho and its contribution to continuous noise. Thus, the dark continuous noise in rods originates mostly, if not exclusively, from rhodopsin holo-pigment.

Rhodopsin-Triggered Continuous Noise Goes through Transducin. If the continuous noise comes from holo-rhodopsin, it should go through $G_{T1}\alpha$. We bred $Rho^{WT/WT};Gcaps^{-/-}$ mice into $Gnat1^{-/-}$ background to eliminate rod transducin. Indeed, the dark continuous noise in $Rho^{WT/WT};Gcaps^{-/-};Gnat1^{-/-}$ rods was much lower (σ^2 = 0.061 ± 0.018 pA^2) (*SI Appendix*, Fig. S2)—close to $Rho^{REY/REY};Gcaps^{-/-}$ rods. The $Gnat1^{-/-}$ background is drastic because the light response disappears, disallowing cell-condition monitoring. We thus checked $Rho^{WT/WT};Gcaps^{-/-};Gnat1^{-/-};Gnat1^{Tg}$ rods, where Gnat1 is expressed transgenically under the rhodopsin promoter in $Gnat1^{-/-}$ background, lowering Gnat1 expression to ~6% of *WT* (35). These mouse rods were similar in continuous noise (σ^2 = 0.058 ± 0.014 pA^2) to $Rho^{REY/REY};Gcaps^{-/-}$ rods and to $Rho^{WT/WT};Gcaps^{-/-};Gnat1^{-/-}$ rods (see above), albeit a normal dark current (Fig. 1*G*; statistics in Fig. 1 *I* and *J*). Conversely, we increased the lifetime of $G_{T1}\alpha^*$ by genetically deleting RGS9, the GTPase-activating protein that accelerates the termination of $G_{T1}\alpha^*$ (37–39). As expected, the amplitude and decay time of the spontaneous-isomerization events of $Rho^{WT/WT};Gcaps^{-/-};RGS9^{-/-}$ rods far exceeded those of $Rho^{WT/WT};Gcaps^{-/-}$ (Fig. 1*H*, note amplitude-scale change). At the same time, the continuous noise of $Rho^{WT/WT};Gcaps^{-/-};RGS9^{-/-}$ rods increased by ~10-fold (σ^2 = 1.539 ± 0.484 pA^2) over $Rho^{WT/WT};Gcaps^{-/-}$and the dark current decreased by ~40% (Fig. 1*I*), due to cumulative continuous noise but not due to the quantal event frequency, which remained at only ~1 event min^{-1}. This behavior of $Rho^{WT/WT};Gcaps^{-/-};RGS9^{-/-}$ rods was mostly removed by the "largely silent" mutant REY-Rho in $Rho^{REY/REY};Gcaps^{-/-};RGS9^{-/-}$ rods, with a significantly decreased continuous noise and a near-normal dark current (*SI Appendix*, Fig. S3). These results again indicate that the continuous-noise source resides in the holo-rhodopsin.

Dark Continuous Noise from Mouse Short-Wavelength Cone Pigment (mOpn1-SW). To examine dark continuous noise from cone pigments, we expressed mOpn1-SW and mouse medium-wavelength cone pigment (mOpn1-MW), as well as human long-wavelength cone pigment (hOpn1-LW), respectively, in mouse rods. For mOpn1-SW and mOpn1-MW, we used the CRISPR method to insert the respective complementary DNA (cDNA) into the rhodopsin gene locus and produced the knock-in (KI) mouse lines, $Rho^{SW/SW}$ and $Rho^{MW/MW}$ (omitting the animal species). For hOpn1-LW, the mouse line ($Opn1\text{-}LW^{Tg}$, with "*Tg*" indicating transgenic) was already available in house (15). As such, a cone pigment's activity could be functionally assessed via its signaling through the high-amplification rod phototransduction pathway (15, 16).

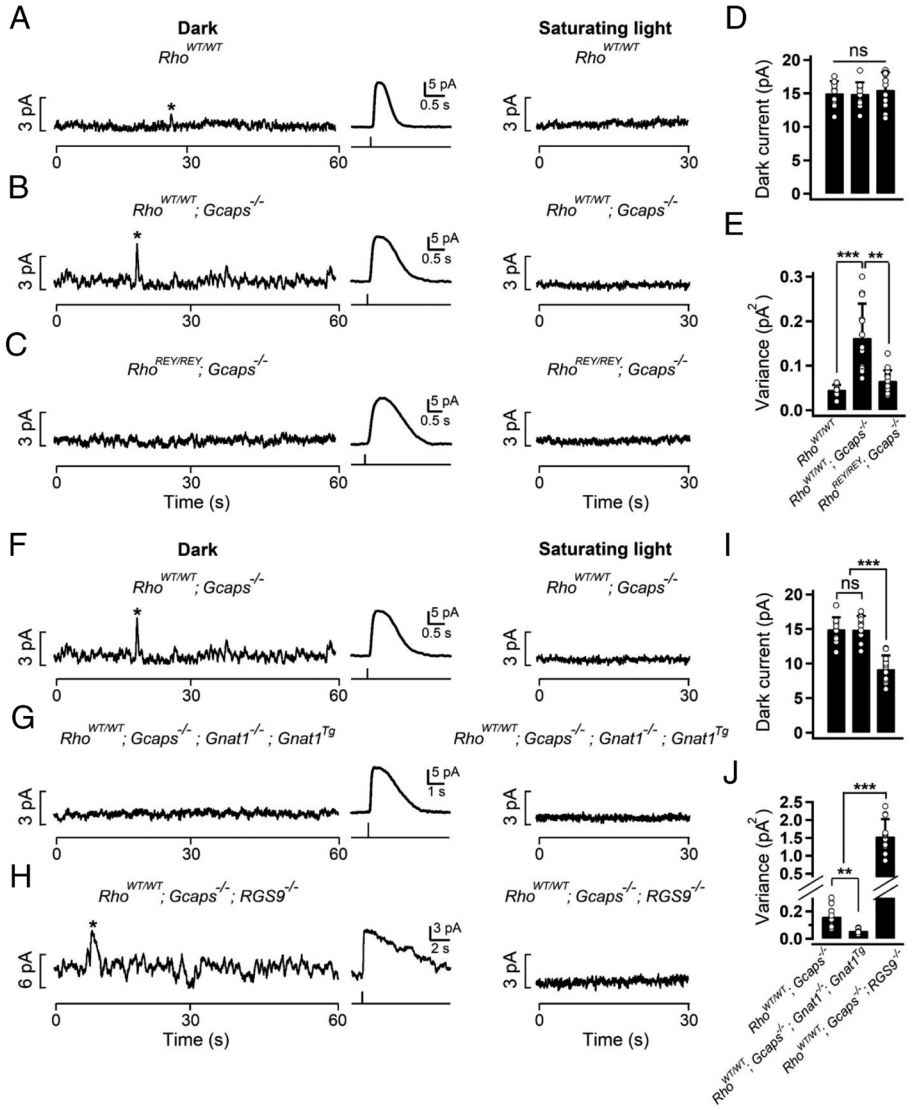

Fig. 1. The dark continuous noise of mouse rods is mostly from rhodopsin and goes through $G_T\alpha$. (*A–C*, *Left*) 60-s stable recordings of dark noise from *Rho*$^{WT/WT}$, *Rho*$^{WT/WT}$;*Gcaps*$^{-/-}$, and *Rho*$^{REY/REY}$;*Gcaps*$^{-/-}$ rods with the spontaneous isomerization labeled with stars. The spontaneous isomerization events of *Rho*$^{REY/REY}$;*Gcaps*$^{-/-}$ rods were too small to be observed. (*Middle*) The saturated light responses of *Rho*$^{WT/WT}$, *Rho*$^{WT/WT}$;*Gcaps*$^{-/-}$, and *Rho*$^{REY/REY}$;*Gcaps*$^{-/-}$ rods to 10-ms, 500-nm flashes. The saturating light intensities were 483, 113, and 509,782 photons μm^{-2} for *Rho*$^{WT/WT}$, *Rho*$^{WT/WT}$;*Gcaps*$^{-/-}$, and *Rho*$^{REY/REY}$;*Gcaps*$^{-/-}$ rods, respectively. (*Right*) 30-s dark noise recordings in saturating light indicating instrumental noise. (*D* and *E*) Statistics showing the dark current and variance of continuous noise in *A–C*. The continuous noise is defined as dark noise without showing any spontaneous isomerization. n = 11 rods for the dark current or variance of *Rho*$^{WT/WT}$, 14 rods for the dark current and 13 rods for the variance of *Rho*$^{WT/WT}$;*Gcaps*$^{-/-}$, 11 rods for the dark current and 18 rods for the variance of *Rho*$^{REY/REY}$;*Gcaps*$^{-/-}$. (*F–J*) The same as *A–E*, except the mouse genotypes were *Rho*$^{WT/WT}$;*Gcaps*$^{-/-}$, *Rho*$^{WT/WT}$;*Gcaps*$^{-/-}$;*Gnat1*$^{-/-}$;*Gnat1*^{Tg}, and *Rho*$^{WT/WT}$;*Gcaps*$^{-/-}$;*RGS9*$^{-/-}$. The saturating light intensities were 113, 483, and 50 photons μm^{-2} at 500 nm for *Rho*$^{WT/WT}$;*Gcaps*$^{-/-}$, *Rho*$^{WT/WT}$;*Gcaps*$^{-/-}$;*Gnat1*$^{-/-}$;*Gnat1*^{Tg}, and *Rho*$^{WT/WT}$;*Gcaps*$^{-/-}$;*RGS9*$^{-/-}$, respectively. n = 14 rods for the dark current and 13 rods for the variance of *Rho*$^{WT/WT}$;*Gcaps*$^{-/-}$, 12 rods for the dark current or variance of *Rho*$^{WT/WT}$;*Gcaps*$^{-/-}$;*Gnat1*$^{-/-}$;*Gnat1*^{Tg}, 14 rods for the dark current and 12 rods for the variance of *Rho*$^{WT/WT}$;*Gcaps*$^{-/-}$;*RGS9*$^{-/-}$. Statistical data were presented as mean ± SD. Statistical significance was analyzed by One-way ANOVA, $^{**}P < 0.01$, $^{***}P < 0.001$; ns, not significant.

We shall start with mOpn1-SW. By breeding the *Rho*$^{SW/SW}$ mouse line with the *Rho*$^{REY/REY}$;*Gcaps*$^{-/-}$ line (35), we obtained *Rho*$^{SW/REY}$;*Gcaps*$^{-/-}$ mice, which have the endogenous WT-Rho replaced by the "largely silenced" REY-Rho in order to isolate the noise from the exogenous cone pigment for monitoring. The action spectrum of *Rho*$^{-/REY}$;*Gcaps*$^{-/-}$ rods measured with dim flashes had a peak around 500 nm (reflecting REY-Rho's λ_{max}), versus two peaks for *Rho*$^{SW/REY}$;*Gcaps*$^{-/-}$ rods, with one perhaps around 360 nm (λ_{max} of mOpn1-SW) and the other around 500 nm (λ_{max} of REY-Rho) (Fig. 2*B*). The limitations of our optics disallowed measurements of dim-flash sensitivity below 360 nm and the response family at 360 nm. However, the significant increase in sensitivity of *Rho*$^{SW/REY}$;*Gcaps*$^{-/-}$ rods around 360 nm compared with *Rho*$^{-/REY}$;*Gcaps*$^{-/-}$ rods (Fig. 2*B*), and the colocalization of mOpn1-SW and rhodopsin in *Rho*$^{SW/REY}$;*Gcaps*$^{-/-}$ rods from immunostaining (Fig. 2*C*) indicated successful expression of mOpn1-SW in *Rho*$^{SW/REY}$;*Gcaps*$^{-/-}$ rods. Given the exceedingly low sensitivity of REY-Rho at 360 nm, it is easy to tell apart the responses from mOpn1-SW and those from REY-Rho in *Rho*$^{SW/REY}$;*Gcaps*$^{-/-}$ rods (Fig. 2*D*). As such, from Poisson analysis of 50 to 100 dim flashes at 360 nm, the single-photon responses from mOpn1-SW and its expression level in *Rho*$^{SW/REY}$;*Gcaps*$^{-/-}$ rods could be evaluated (*Materials and Methods*). We obtained a single-photon response of 1.76 ± 0.52 pA from mOpn1-SW when expressed in rods and 0.15 ± 0.04 pA from REY-Rho (Fig. 2*E* and *SI Appendix*, Table S1) (versus our previously obtained 2.9 ± 1.5 pA from WT-Rho in *Gcaps*$^{-/-}$ background, 36). Importantly, the amount of mOpn1-SW expressed

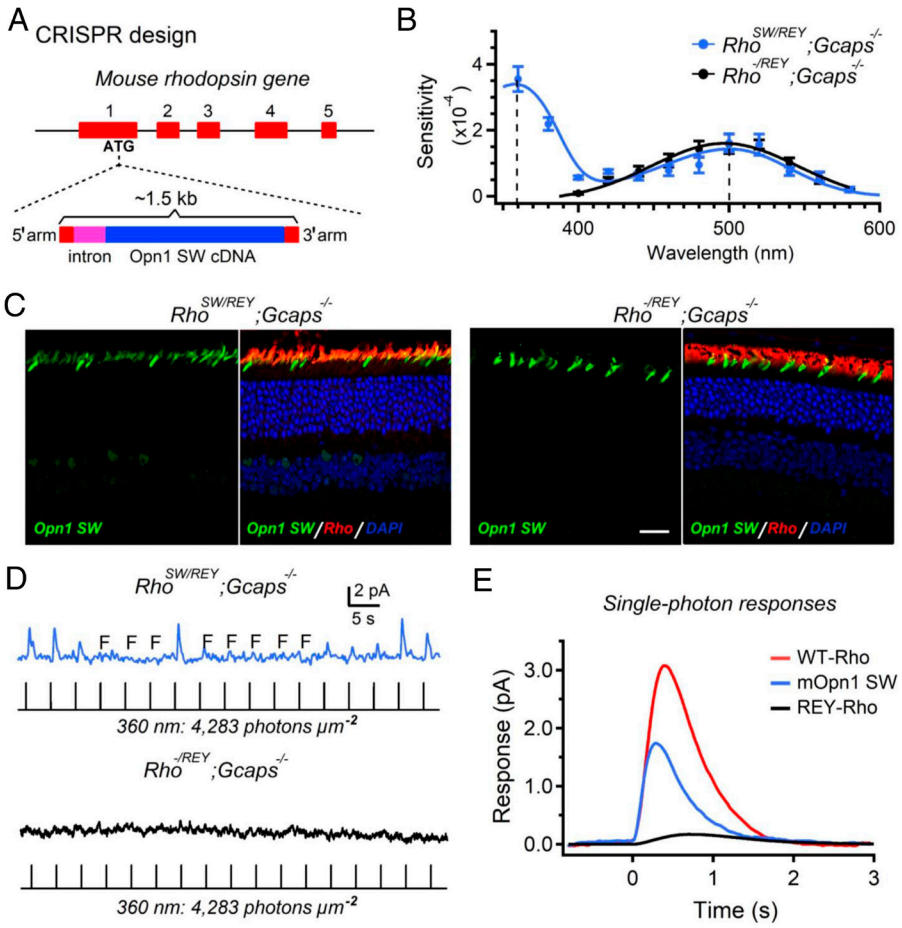

Fig. 2. Characterization of mouse Opn1-SW-KI mouse line. (*A*) A diagram showing the CRISPR design for making the mouse Opn1-SW-KI mouse line. A ~1.5 kb cDNA fragment was inserted at the start codon of rhodopsin, thus the rhodopsin allele is replaced by mouse Opn1-SW. (*B*) Action spectra of *Rho*$^{SW/REY}$;*Gcaps*$^{-/-}$ (blue) and *Rho*$^{-/REY}$;*Gcaps*$^{-/-}$ (black) rods were determined by measuring the dim-flash sensitivities at different wavelengths. (*C*) Immunostaining for the mouse Opn1-SW (green) and rhodopsin (red) of *Rho*$^{SW/REY}$;*Gcaps*$^{-/-}$ and *Rho*$^{-/REY}$;*Gcaps*$^{-/-}$ retinae. DAPI (blue) was used to indicate the nuclei of cells. The colocalization of mouse Opn1-SW and rhodopsin in *Rho*$^{SW/REY}$;*Gcaps*$^{-/-}$ rods, but not in *Rho*$^{-/REY}$;*Gcaps*$^{-/-}$ rods indicates the successful expression of mouse Opn1-SW in the KI rods. (Scale bars, 20 µm.) (*D*) Flash responses of a *Rho*$^{SW/REY}$;*Gcaps*$^{-/-}$ rod (blue) and a *Rho*$^{-/REY}$;*Gcaps*$^{-/-}$ rod (black) to repetitive 10-ms, 360-nm flashes at 4,283 photons µm^{-2}. Stimuli that failed to elicit responses were labeled as "F" (a failure was defined as a flash trial that did not result in a response reaching a criterion amplitude, typically ≥50% of the single-photon-response peak within a characteristic time window based on the average response waveform). No failure could be recognized for *Rho*$^{-/REY}$;*Gcaps*$^{-/-}$ rods because of their small single-photon responses. (*E*) The averaged single-photon responses of *Rho*$^{WT/WT}$;*Gcaps*$^{-/-}$ (red), *Rho*$^{SW/REY}$;*Gcaps*$^{-/-}$ (blue) and *Rho*$^{-/REY}$;*Gcaps*$^{-/-}$ (black) rods. n = 23 rods for *Rho*$^{WT/WT}$;*Gcaps*$^{-/-}$, 12 rods for *Rho*$^{SW/REY}$;*Gcaps*$^{-/-}$ and 9 rods for *Rho*$^{-/REY}$;*Gcaps*$^{-/-}$.

in the *Rho*$^{SW/REY}$;*Gcaps*$^{-/-}$ rods was calculated from the probability of failure in the dim-flash responses series (*Materials and Methods*) to be ~0.057% of WT-Rho in *Rho*$^{WT/WT}$;*Gcaps*$^{-/-}$ rods. Next, we recorded dark noise from *Rho*$^{SW/REY}$;*Gcaps*$^{-/-}$ and *Rho*$^{-/REY}$;*Gcaps*$^{-/-}$ rods. Consistent with previous study (36), *Rho*$^{-/REY}$;*Gcaps*$^{-/-}$ rods showed no visible events because of the small single-photon responses (see above) (Fig. 3 *A*, *Right*). For *Rho*$^{SW/REY}$;*Gcaps*$^{-/-}$ rods, the spontaneous isomerization rate was ~1 event per 6.7 min with a probability of occurrence obeying Poisson statistics (Fig. 3 *A*, *Left* and Fig. 3*C*). Importantly, the dark continuous noise of *Rho*$^{SW/REY}$;*Gcaps*$^{-/-}$ rods (σ^2 = 0.169 ± 0.058 pA^2) was significantly larger than that of *Rho*$^{-/REY}$;*Gcaps*$^{-/-}$ (σ^2 = 0.069 ± 0.018 pA^2), albeit with similar dark currents (Fig. 3 *B*, *D*, and *E*), giving $\Delta\sigma^2$ = 0.1 pA^2, reflecting continuous noise from mOpn1-SW. To exclude possible noise contribution from apo-opsin, we applied 11-*cis*-retinal to *Rho*$^{SW/REY}$;*Gcaps*$^{-/-}$ rods but found no change in continuous noise and dark current (*SI Appendix*, Fig. S4 *A* and *B*).

Dark Continuous Noise from mOpn1-MW. We repeated the same measurements as above on *Rho*$^{MW/REY}$;*Gcaps*$^{-/-}$ rods. The action spectrum of *Rho*$^{MW/REY}$;*Gcaps*$^{-/-}$ rods measured with dim flashes had a λ_{max} at ~510 nm (near to mOpn1-MW) (Fig. 4*B*). The presence of mOpn1-MW in *Rho*$^{MW/REY}$;*Gcaps*$^{-/-}$ rods was confirmed by immunolabeling (Fig. 4*C*). Based on flash response families at 500 nm (Fig. 4*D*) (with corresponding flash-response relations shown in Fig. 4*E*), *Rho*$^{MW/REY}$;*Gcaps*$^{-/-}$ rods were ~7.6-fold more sensitive than *Rho*$^{-/REY}$;*Gcaps*$^{-/-}$ rods, and at <10,000 photons µm^{-2}, λ = 500 nm the response came predominantly from mOpn1-MW (Fig. 4*F*). With 50 to 100 dim flashes at 500 nm, the single-photon response from mOpn1-MW and its expression level in *Rho*$^{MW/REY}$;*Gcaps*$^{-/-}$ rods could be evaluated. Interestingly, both the single-photon response (1.44 ± 0.47 pA) and the expression level (~0.055% of WT-Rho in *Rho*$^{WT/WT}$;*Gcaps*$^{-/-}$ rods) of mOpn1-MW in *Rho*$^{MW/REY}$;*Gcaps*$^{-/-}$ rods were quite similar to the mOpn1-SW in *Rho*$^{SW/REY}$;*Gcaps*$^{-/-}$ rods (Fig. 4*G* and *SI Appendix*, Table S1). The cellular rate of spontaneous isomerization of mOpn1-MW in *Rho*$^{MW/REY}$;*Gcaps*$^{-/-}$ rods was ~1 event per 26 min with a probability of occurrence obeying Poisson statistics (Fig. 5 *A* and *C*). The continuous-noise variance in *Rho*$^{MW/REY}$;*Gcaps*$^{-/-}$ rods was also larger than in *Rho*$^{-/REY}$;*Gcaps*$^{-/-}$ rods (σ^2 = 0.124 ± 0.044 pA^2 for *Rho*$^{MW/REY}$;*Gcaps*$^{-/-}$ and σ^2 = 0.069 ± 0.018 for *Rho*$^{-/REY}$;*Gcaps*$^{-/-}$; see earlier) with similar dark currents (Fig. 5 *B*, *D*, and *E*), giving $\Delta\sigma^2$ = 0.055 pA^2, reflecting continuous noise from mOpn1-MW. To exclude possible noise

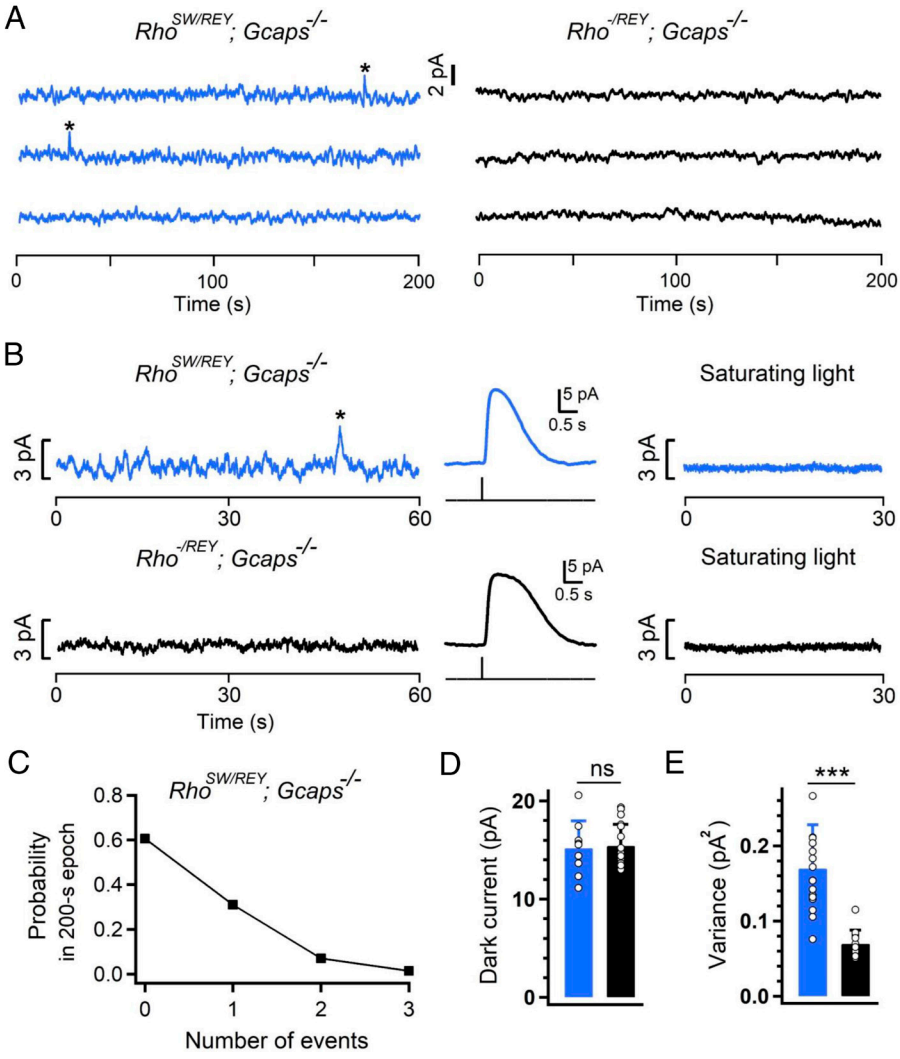

Fig. 3. Dark noise from *Rho*$^{SW/REY}$;*Gcaps*$^{-/-}$ rods. (*A*) 10-min dark noise recordings for *Rho*$^{SW/REY}$;*Gcaps*$^{-/-}$ rods (blue) and *Rho*$^{-/REY}$;*Gcaps*$^{-/-}$ (black) rods. (*B*, *Left*) 60-s dark noise recordings from *Rho*$^{SW/REY}$;*Gcaps*$^{-/-}$ rods (blue) and *Rho*$^{-/REY}$;*Gcaps*$^{-/-}$ (black) rods. (*Middle*) Saturated light responses to 10-ms flashes from *Rho*$^{SW/REY}$;*Gcaps*$^{-/-}$ rods (blue) and *Rho*$^{-/REY}$;*Gcaps*$^{-/-}$ rods (black). The saturating light intensities were 970,458 photons μm^{-2} at 440 nm for *Rho*$^{SW/REY}$;*Gcaps*$^{-/-}$ rods (blue) and 1,144,692 photons μm^{-2} at 500 nm for *Rho*$^{-/REY}$;*Gcaps*$^{-/-}$ rods (black). For *Rho*$^{SW/REY}$;*Gcaps*$^{-/-}$ rods, we had to use 440 nm light for the saturated responses because of our optical limits in UV light. (*Right*) 30-s dark-noise recordings in saturating light indicating instrumental noise. (*C*) Poisson analysis of the spontaneous isomerization events collected from all *Rho*$^{SW/REY}$;*Gcaps*$^{-/-}$ rods. The probability of 0, 1, 2, and 3 events observed in a total of 71 trials of 200-s epochs is plotted as the square symbols. The solid line shows very good fit by the Poisson distribution with a mean event rate of 0.00245 s^{-1}. (*D* and *E*) Statistics showing the dark current and variance of continuous noise of *Rho*$^{SW/REY}$;*Gcaps*$^{-/-}$ and *Rho*$^{-/REY}$;*Gcaps*$^{-/-}$ rods. n = 9 rods for the dark current and 17 rods for the variance of *Rho*$^{SW/REY}$;*Gcaps*$^{-/-}$, 17 rods for the dark current and 12 rods for the variance of *Rho*$^{-/REY}$;*Gcaps*$^{-/-}$ rods. Statistical data were presented as mean ± SD. Statistical significance was analyzed by Student's *t* test, ***P < 0.001; ns, not significant.

from apo-opsin, we applied 11-*cis*-retinal to *Rho*$^{MW/REY}$;*Gcaps*$^{-/-}$ rods but again found no change in continuous noise and dark current (*SI Appendix*, Fig. S4 *C* and *D*).

Dark Continuous Noise from hOpn1-LW. In the same manner, we measured the continuous noise from human L-cone pigment in the *Opn1-LW*^{Tg} transgenic mouse line after crossing it with the *Rho*$^{REY/REY}$;*Gcaps*$^{-/-}$ line (*Opn1-LW*^{Tg};*Rho*$^{REY/REY}$;*Gcaps*$^{-/-}$). The transgenic mouse line has been validated previously (15), so we did not repeat the action spectrum experiment here. However, our immunostaining did confirm the expression of Opn1-LW in the transgenic rods (*SI Appendix*, Fig. S5). We then collected 50 to 100 dim flashes at 560 nm (near λ_{max} of hOpn1-LW) and found that the single-photon responses from hOpn1-LW in *Opn1-LW*^{Tg};*Rho*$^{REY/REY}$;*Gcaps*$^{-/-}$ rods was 1.86 ± 0.45 pA and the expression level of hOpn1-LW was ~0.02% of WT-Rho in *Rho*$^{WT/WT}$;*Gcaps*$^{-/-}$ rods (Fig. 6 *A* and *B* and *SI Appendix*, Table S1). This level of hOpn1-LW was about 10-fold lower than what we reported previously (15), probably due to the progressive loss of hOpn1-LW transgene over many generations in ~15 y. Consistent with the lower expression level of hOpn1-LW, the cellular rate of the spontaneous isomerization event was correspondingly lower than our previous report (Fig. 6 *C* and *D*, ~1 event per 7.2 min in this study versus ~1 event per 0.8 min in our previous study; see ref. 15). We next measured the continuous noise of *Opn1-LW*^{Tg};*Rho*$^{REY/REY}$;*Gcaps*$^{-/-}$ rods and found this to be significantly higher than in *Rho*$^{REY/REY}$;*Gcaps*$^{-/-}$ rods (Fig. 6*E*, σ^2 = 0.165 ± 0.065 pA^2 for *Opn1-LW*^{Tg};*Rho*$^{REY/REY}$;*Gcaps*$^{-/-}$ and σ^2 = 0.066 ± 0.024 pA^2 for *Rho*$^{REY/REY}$;*Gcaps*$^{-/-}$), giving $\Delta\sigma^2$ = 0.099 pA^2, reflecting continuous noise from hOpn1-LW, again not changed with addition of 11-*cis*-retinal (*SI Appendix*, Fig. S4 *E* and *F*).

Quantification of Dark Continuous Noise from Rhodopsin and Cone Pigments. Compared to WT-Rho in *Rho*$^{WT/WT}$;*Gcaps*$^{-/-}$ rods, the respective expression level of mOpn1-SW in *Rho*$^{SW/REY}$;*Gcaps*$^{-/-}$ rods was ~0.057%, of mOpn1-MW in *Rho*$^{MW/REY}$;*Gcaps*$^{-/-}$ rods was

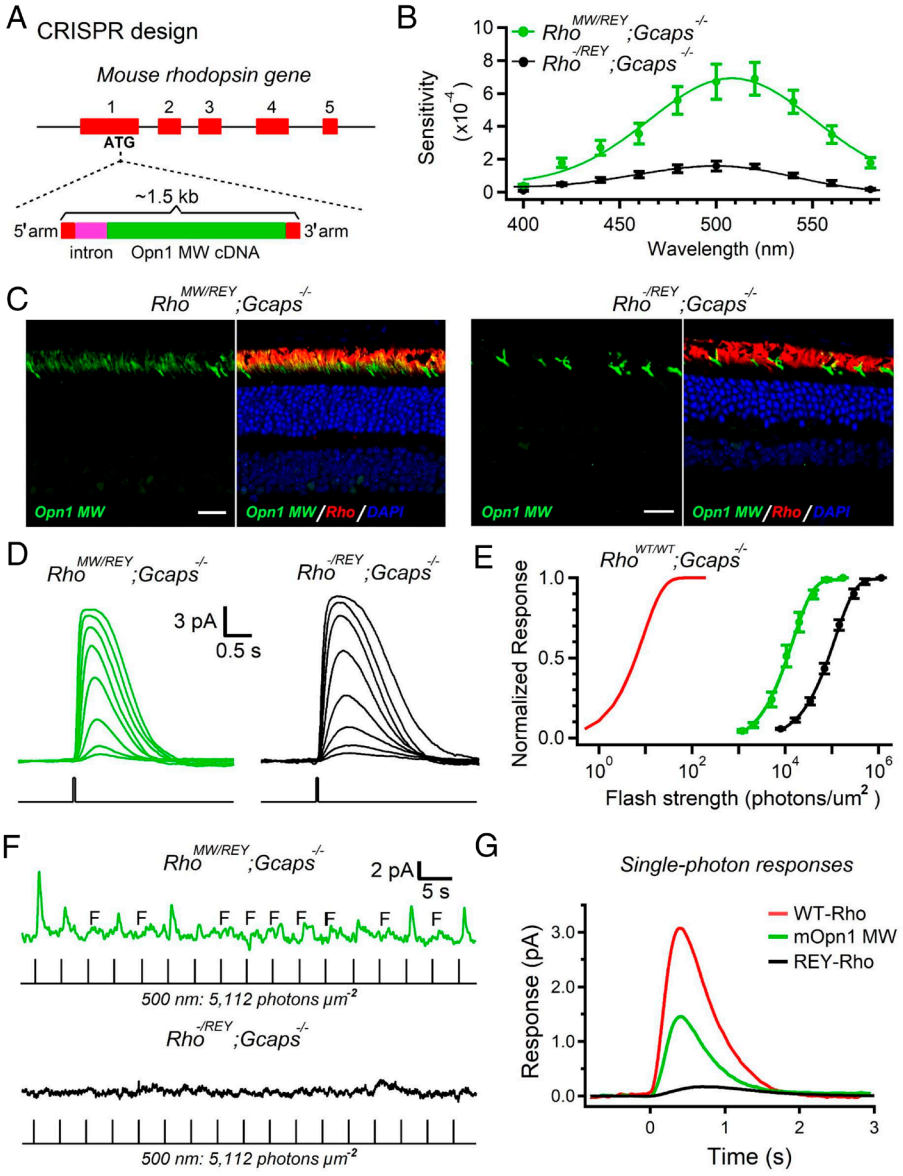

Fig. 4. Characterization of mouse Opn1-MW-KI mouse line. (*A*) A diagram showing the CRISPR design for making the mouse Opn1-MW-KI mouse line. A ~1.5 kb cDNA fragment was inserted at the start codon of rhodopsin, thus the rhodopsin allele was replaced by mouse Opn1-MW. (*B*) Action spectra of *Rho*$^{MW/REY}$;*Gcaps*$^{-/-}$ (green) and *Rho*$^{-/REY}$;*Gcaps*$^{-/-}$ (black) rods were determined by measuring the dim-flash sensitivities at different wavelengths. (*C*) Immunostaining for the mouse Opn1-MW (green) and rhodopsin (red) of *Rho*$^{MW/REY}$;*Gcaps*$^{-/-}$ and *Rho*$^{-/REY}$;*Gcaps*$^{-/-}$ retinae. DAPI (blue) was used to indicate the nuclei of cells. The colocalization of mouse Opn1-MW and rhodopsin in *Rho*$^{MW/REY}$;*Gcaps*$^{-/-}$ rods, but not in *Rho*$^{-/REY}$;*Gcaps*$^{-/-}$ rods, indicates the successful expression of mouse Opn1-MW in the KI rods. (Scale bars, 20 µm.) (*D* and *E*) Averaged flash-response families to 10-ms, 500 nm flashes at different light intensities and the intensity–response relations from 12 *Rho*$^{MW/REY}$;*Gcaps*$^{-/-}$ rods (green) and 9 *Rho*$^{-/REY}$;*Gcaps*$^{-/-}$ rods (black). The red curve in *E* is the intensity–response relation from *Rho*$^{WT/WT}$;*Gcaps*$^{-/-}$ rods obtained from our previous study (35). The intensity–response relations were fitted with a single saturating-exponential function giving half-saturating flash strengths of 6.21, 11,256, and 85,392 photons µm^{-2} for *Rho*$^{WT/WT}$;*Gcaps*$^{-/-}$ (red), *Rho*$^{MW/REY}$;*Gcaps*$^{-/-}$ (green) and *Rho*$^{-/REY}$;*Gcaps*$^{-/-}$ (black) rods, respectively. (*F*) Flash responses of a *Rho*$^{MW/REY}$;*Gcaps*$^{-/-}$ rod (green) and a *Rho*$^{-/REY}$;*Gcaps*$^{-/-}$ rod (black) to repetitive 10-ms, 500 nm flashes at 5,112 photons µm^{-2}. Stimuli that failed to elicit responses were labeled as F (a failure was defined as a flash trial that did not result in a response reaching a criterion amplitude, typically ≥50% of the single-photon-response peak within a characteristic time window based on the average response waveform). No failure was recognized for *Rho*$^{-/REY}$;*Gcaps*$^{-/-}$ rods because of its small single-photon responses. (*G*) The average single-photon responses of *Rho*$^{WT/WT}$;*Gcaps*$^{-/-}$ (red), *Rho*$^{MW/REY}$;*Gcaps*$^{-/-}$ (green) and *Rho*$^{-/REY}$;*Gcaps*$^{-/-}$ (black) rods. n = 23 rods for *Rho*$^{WT/WT}$;*Gcaps*$^{-/-}$, 23 rods for *Rho*$^{MW/REY}$; *Gcaps*$^{-/-}$ and 9 rods for *Rho*$^{-/REY}$; *Gcaps*$^{-/-}$.

~0.055%, and of hOpn1-LW in *Opn1-LW*^{Tg};*Rho*$^{REY/REY}$;*Gcaps*$^{-/-}$ rods was ~0.02%. These levels were all under 0.1% of the normal expression of WT-Rho in rods. However, the variance associated with the dark continuous noise in all four genotypes were comparable: σ^2 = 0.162 ± 0.077 pA^2 for *Rho*$^{WT/WT}$;*Gcaps*$^{-/-}$ rods, 0.169 ± 0.058 pA^2 for *Rho*$^{SW/REY}$;*Gcaps*$^{-/-}$ rods, 0.124 ± 0.044 pA^2 for *Rho*$^{MW/REY}$;*Gcaps*$^{-/-}$ rods, and 0.165 ± 0.065 pA^2 for *Opn1-LW*^{Tg};*Rho*$^{REY/REY}$;*Gcaps*$^{-/-}$ rods, indicating a much higher event rate of continuous noise from the three cone pigments. To further quantify the dark continuous noise from rhodopsin and cone pigments, and to compare with their corresponding spontaneous isomerization noise, we made use of Campbell's Theorems (35, 40). We shall start with rhodopsin-triggered continuous noise as an example. Because the holo-rhodopsin-driven dark continuous noise goes through $G_{T1}\alpha$ as described earlier, the successful unitary event should be representable by the response evoked by a single $G_{T1}\alpha$*-PDE* complex, essentially the same as the electrical response produced by a single transiently active apo-opsin molecule (35). Previously, we obtained the power spectrum of the latter from the dark continuous noise associated with apo-opsin produced after a bleach, describable by a convolution of two single-exponential declines, with time constants of τ_1 = 81 ± 35 ms,

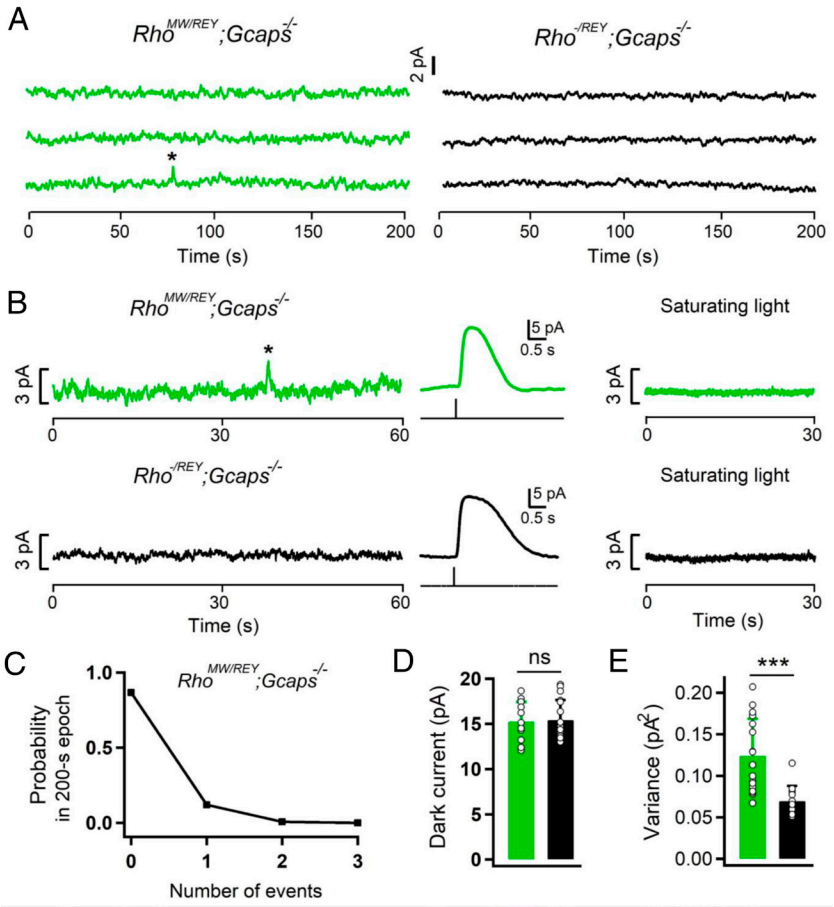

Fig. 5. Dark noise from *Rho*$^{MW/REY}$;*Gcaps*$^{-/-}$rods. (*A*) 10-min dark-noise recordings from *Rho*$^{MW/REY}$;*Gcaps*$^{-/-}$ (green) and *Rho*$^{-/REY}$;*Gcaps*$^{-/-}$ (black) rods. (*B*, *Left*) 60-s dark-noise recordings from *Rho*$^{MW/REY}$;*Gcaps*$^{-/-}$ (green) and *Rho*$^{-/REY}$;*Gcaps*$^{-/-}$ (black) rods. (*Middle*) Saturated light responses to 10-ms, 500-nm flashes from *Rho*$^{MW/REY}$;*Gcaps*$^{-/-}$ (green) and *Rho*$^{-/REY}$;*Gcaps*$^{-/-}$ (black) rods. The saturating light intensities were 171,726 and 1,144,692 photons μm^{-2} at 500 nm for *Rho*$^{MW/REY}$;*Gcaps*$^{-/-}$ and *Rho*$^{-/REY}$;*Gcaps*$^{-/-}$ rods, respectively. (*Right*) 30-s dark noise recordings in saturating light indicating instrumental noise. (*C*) Poisson analysis of the spontaneous isomerization events collected from all *Rho*$^{MW/REY}$;*Gcaps*$^{-/-}$ rods. The probability of 0, 1, 2, and 3 events observed in a total of 150 trials of 200-s epochs is plotted as the square symbols. The solid lines show very good fit by the Poisson distribution with a mean event rate of 0.00065 s^{-1}. (*D* and *E*) Statistics showing the dark current and variance of continuous noise from *Rho*$^{MW/REY}$;*Gcaps*$^{-/-}$ (green) and *Rho*$^{-/REY}$;*Gcaps*$^{-/-}$ (black) rods. n = 12 rods for the dark current and 19 rods for the variance of *Rho*$^{MW/REY}$;*Gcaps*$^{-/-}$, 17 rods for the dark current and 12 rods for the variance of *Rho*$^{-/REY}$;*Gcaps*$^{-/-}$ rods. Statistical data were presented as mean ± SD. Statistical significance was analyzed by Student's *t* test, ***$P < 0.001$; ns, not significant.

τ_2 = 231 ± 25 ms (35). As such, by calculating the power spectra of the continuous noise in *Rho*$^{WT/WT}$;*Gcaps*$^{-/-}$ rods and *Rho*$^{REY/REY}$;*Gcaps*$^{-/-}$ rods, and taking the difference (difference spectrum) between them, we found the result to indeed match that of the single apo-opsin activity (Fig. 7 *A* and *B*). Thus, the activity underlying the dark continuous noise triggered by WT-Rho is identical in waveform to that triggered by apo-opsin after a bleach, with each being the unitary G_{T1}α*-PDE* response.

Next, we compared the spontaneous-isomerization noise with the continuous noise from WT-Rho. For unitary events with waveform *f(t)* occurring randomly at a mean rate of ν s^{-1}, the mean and the variance of the steady signal resulting from such events are given by Campbell's Theorems:

$$\text{Steady noise mean (m)} = \nu \int f(t)dt, \qquad [1]$$

$$\text{Steady noise variance } (\sigma^2) = \nu \int \left[f(t)\right]^2 dt. \qquad [2]$$

We first consider WT-Rho-triggered spontaneous isomerization. For *Rho*$^{WT/WT}$;*Gcaps*$^{-/-}$ rods, the average spontaneous isomerization rate is 0.52 ± 0.26 event min^{-1} (see above), namely 0.0087 ± 0.0043 R* s^{-1} cell^{-1}. Applying Eq. **1**, the steady noise mean, m_i (where subscript "*i*" denotes isomerization) from WT-Rho-triggered isomerization noise is thus given by $m_i = \nu_i \int f_i(t)dt$ = 0.0087 s^{-1} × 1.82 pC ~0.016 pA, where $\int f_i(t)dt = 1.82$pC is the time integral of single-photon responses from WT-Rho in *Rho*$^{WT/WT}$;*Gcaps*$^{-/-}$ rods (*SI Appendix*, Table S1).

We next consider WT-Rho-triggered dark continuous noise. Our previous work on dark continuous noise after a bleach has provided the waveform kinetics (see earlier) as well as the transient peak amplitude (0.27 pA, the average in different bleaching conditions) of the response evoked by a single G_{T1}α*-PDE* complex (35). Thus, $\int f_c(t)dt$ (where subscript "*c*" denotes the unit underlying the continuous noise), the time integral of the unitary event can be obtained to be 0.12 pC, and $\int \left[f_c(t)\right]^2 dt$ calculated to be 0.021 pA^2 s after averaging values under different bleaching conditions (35). Next, between the *Rho*$^{WT/WT}$;*Gcaps*$^{-/-}$ and *Rho*$^{REY/REY}$;*Gcaps*$^{-/-}$ genotypes, their difference in continuous-noise variance gave the WT-Rho-triggered continuous-noise variance, $\sigma_c^2 = \sigma^2_{Rho^{WT/WT};Gcaps^{-/-}} - \sigma^2_{Rho^{REY/REY};Gcaps^{-/-}}$ = 0.162 pA^2 – 0.066 pA^2 = 0.096 pA^2. Applying Eq. **2**, the frequency, ν_c, of unitary events comprising WT-Rho continuous noise is thus given by $\nu_c = \sigma_c^2 / \left\{\int [f_c(t)]^2 dt\right\}$ = 0.096 pA^2/0.021 pA^2 s ~ 4.57 s^{-1}. Inserting this ν_c value into Eq. **1**, we obtained the steady noise

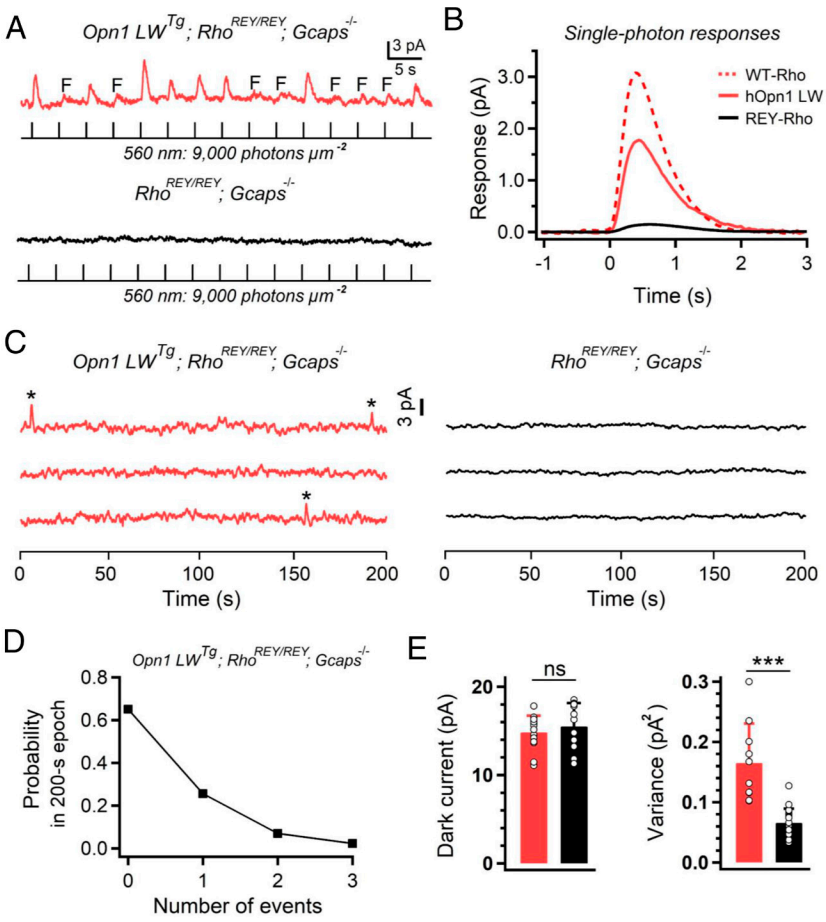

Fig. 6. Dark continuous noise from *Opn1-LW^{Tg};Rho$^{REY/REY}$;Gcaps$^{-/-}$*transgenic rods. (*A*) Responses of a *Opn1-LW^{Tg};Rho$^{REY/REY}$;Gcaps$^{-/-}$* rod (red) and a *Rho$^{REY/REY}$;Gcaps$^{-/-}$* rod (black) to repetitive 10-ms, 560-nm flashes at 9,000 photons μm^{-2}. Stimuli that failed to elicit responses were labeled as F. No failure was recognized for *Rho$^{REY/REY}$;Gcaps$^{-/-}$* rods because of its small single-photon responses. (*B*) The averaged single-photon responses of *Rho$^{WT/WT}$;Gcaps$^{-/-}$* (dashed red), *Opn1-LW^{Tg};Rho$^{REY/REY}$;Gcaps$^{-/-}$* (solid red) and *Rho$^{REY/REY}$;Gcaps$^{-/-}$* (black) rods. n = 23 rods for *Rho$^{WT/WT}$;Gcaps$^{-/-}$*, 10 rods for *Opn1-LW^{Tg};Rho$^{REY/REY}$;Gcaps$^{-/-}$* and 9 rods for *Rho$^{REY/REY}$;Gcaps$^{-/-}$*. (*C*) A 10-min dark-noise recording from *Opn1-LW^{Tg};Rho$^{REY/REY}$;Gcaps$^{-/-}$* (red) and *Rho$^{REY/REY}$;Gcaps$^{-/-}$* (black) rods. (*D*) Poisson analysis of the spontaneous isomerization events collected from all *Opn1-LW^{Tg};Rho$^{REY/REY}$;Gcaps$^{-/-}$* rods. The probability of 0, 1, 2, and 3 events observed in a total of 43 trials of 200-s epochs is plotted as the square symbols. The solid line shows very good fit by the Poisson distribution with a mean event rate of 0.00235 s^{-1}. (*E*) Statistics showing the dark current and variance of continuous noise of *Opn1-LW^{Tg};Rho$^{REY/REY}$;Gcaps$^{-/-}$* and *Rho$^{REY/REY}$;Gcaps$^{-/-}$* rods. n = 14 rods for the dark current and 10 rods for the variance of *Opn1-LW^{Tg};Rho$^{REY/REY}$;Gcaps$^{-/-}$*, 11 rods for the dark current and 18 rods for the variance of *Rho$^{REY/REY}$;Gcaps$^{-/-}$* rods. Statistical data were presented as mean ± SD. Statistical significance was analyzed by Student's *t* test, ***$P < 0.001$; ns, not significant.

mean for WT-Rho-triggered continuous noise, $m_c = \nu_c \int f_c(t)dt$ = 4.57 s^{-1} × 0.12 pC ~ 0.55 pA. Thus, in terms of the mean steady signal, WT-Rho-triggered continuous noise is m_c/m_i = 0.55 pA/0.016 pA ~34-fold as high as the spontaneous isomerization. Converting into units of R* s^{-1}, this is equivalent to 34 × 0.0087 R* s^{-1} cell^{-1} = ~0.30 R* s^{-1} cell^{-1} in WT rods.

One can repeat the same data analysis as above for the cone pigments: mOpn1-SW, mOpn1-MW, and hOpn1-LW. As such, by subtracting the power spectrum of *Rho$^{-/REY}$;Gcaps$^{-/-}$* rods from that of *Rho$^{SW/REY}$;Gcaps$^{-/-}$* and *Rho$^{MW/REY}$;Gcaps$^{-/-}$* rods (Fig. 7 *C–E*, *G*, and *H*), and subtracting the power spectrum of *Rho$^{REY/REY}$;Gcaps$^{-/-}$* rods from *Opn1-LW^{Tg};Rho$^{REY/REY}$;Gcaps$^{-/-}$* rods (Fig. 7 *A*, *F*, and *I*), we obtained the power spectra for the mOpn1-SW-, mOpn1-MW-, and hOpn1-LW-triggered continuous noise, respectively. These difference spectra were fitted fairly well by the waveform of unitary G_{T1}α*-PDE* (Fig. 7 *G–I*), indicating that the unitary events underlying mOpn1-SW-, mOpn1-MW-, and hOpn1-LW-triggered continuous noise were also single G_{T1}α*-PDE* response. We then quantified the spontaneous-isomerization noise and continuous noise from mOpn1-SW, mOpn1-MW, and hOpn1-LW as above. Our final calculations (see *SI Appendix, Supplementary Text* for details) showed that mOpn1-SW-triggered continuous noise is ~204-fold as high as the spontaneous isomerization (1 event per 6.7 min) and equivalent to ~0.51 R* s^{-1} cell^{-1} in *Rho$^{SW/REY}$;Gcaps$^{-/-}$* rods with ~0.057% of mOpn1-SW expressed. mOpn1-MW-triggered continuous noise is ~517-fold as high as the spontaneous isomerization (1 event per 26 min), and equivalent to ~0.33 R* s^{-1} cell^{-1} in *Rho$^{MW/REY}$;Gcaps$^{-/-}$* rods with ~0.055% of mOpn1-MW expressed. Finally, hOpn1-LW-triggered continuous noise is ~162-fold as high as the spontaneous isomerization (1 event per 7.2 min), and equivalent to ~0.37 R* s^{-1} cell^{-1} in *Opn1-LW^{Tg};Rho$^{REY/REY}$;Gcaps$^{-/-}$* rods with ~0.02% of hOpn1-LW expressed. Thus, 100% mOpn1-SW would generate ~4.4 R* s^{-1} cell^{-1} for spontaneous-isomerization noise and equivalent to ~895 R* s^{-1} cell^{-1} for continuous noise, and 100% mOpn1-MW would generate ~1.2 R* s^{-1} cell^{-1} for spontaneous-isomerization noise and equivalent to ~600 R* s^{-1} cell^{-1} for continuous noise. Finally, 100% hOpn1-LW would generate ~11.4 R* s^{-1} cell^{-1} for spontaneous-isomerization noise and equivalent to ~1,850 R* s^{-1} cell^{-1} for continuous noise.

Discussion

Visual pigments in rods and cones are known to exhibit spontaneous isomerization (quantal noise) in darkness triggered by intramolecular thermal energy (6–8). The electrical consequence of

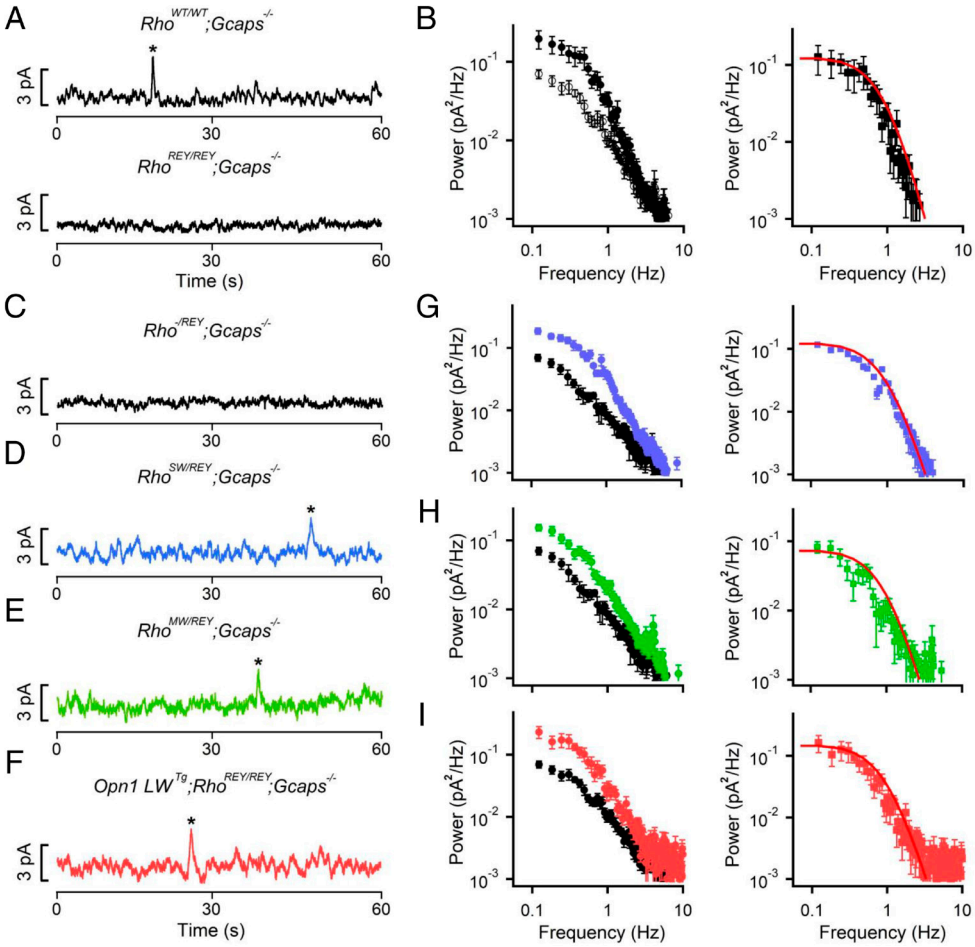

Fig. 7. Quantification of dark continuous noise from rhodopsin and cone pigments. (*A*) 60-s dark-noise recordings from a $Rho^{WT/WT};Gcaps^{-/-}$ (*Upper*) and $Rho^{REY/REY};Gcaps^{-/-}$ (*Lower*) rods. (*B*, *Left*) Averaged continuous-noise power spectra from $Rho^{WT/WT};Gcaps^{-/-}$ (closed circles) and $Rho^{REY/REY};Gcaps^{-/-}$ rods (open circles). Each frequency point indicates mean ± SEM (n = 10 rods for $Rho^{WT/WT};Gcaps^{-/-}$, 12 rods for $Rho^{REY/REY};Gcaps^{-/-}$). (*Right*) Difference spectrum obtained by subtracting the spectrum of $Rho^{REY/REY};Gcaps^{-/-}$ rods from the spectrum of $Rho^{WT/WT};Gcaps^{-/-}$ rods was fitted by the waveform of single-transducin response (red curve). (*C–F*) 60-s dark-noise recordings from $Rho^{-/REY};Gcaps^{-/-}$ (black), $Rho^{SW/REY};Gcaps^{-/-}$ (blue), $Rho^{MW/REY};Gcaps^{-/-}$ (green) and $Opn1\text{-}LW^{Tg};Rho^{REY/REY};Gcaps^{-/-}$ (red) rods. (*G*, *Left*) averaged continuous-noise power spectra from $Rho^{SW/REY};Gcaps^{-/-}$ (blue) and $Rho^{-/REY};Gcaps^{-/-}$ (black) rods. Each frequency point indicates mean ± SEM (n = 12 rods for $Rho^{-/REY};Gcaps^{-/-}$ and 16 rods for $Rho^{SW/REY};Gcaps^{-/-}$). (*Right*) difference spectrum obtained by subtracting the spectrum of $Rho^{-/REY};Gcaps^{-/-}$ rods from the spectrum of $Rho^{SW/REY};Gcaps^{-/-}$ rods was fitted by the waveform of single transducin response (red curve). (*H*, *Left*) averaged continuous-noise power spectra from $Rho^{MW/REY};Gcaps^{-/-}$ (green) and $Rho^{-/REY};Gcaps^{-/-}$ (black) rods. Each frequency point indicates mean ± SEM (n = 12 rods for $Rho^{-/REY};Gcaps^{-/-}$ or $Rho^{MW/REY};Gcaps^{-/-}$). (*Right*) Difference spectrum obtained by subtracting the spectrum of $Rho^{-/REY};Gcaps^{-/-}$ rods from the spectrum of $Rho^{MW/REY};Gcaps^{-/-}$ rods was fitted by the waveform of single transducin response (red curve). (*I*, *Left*) averaged continuous-noise power spectra from $Opn1\text{-}LW^{Tg};Rho^{REY/REY};Gcaps^{-/-}$ (red) and $Rho^{REY/REY};Gcaps^{-/-}$ (black) rods. Each frequency point indicates mean ± SEM (n = 12 rods for $Rho^{REY/REY};Gcaps^{-/-}$ and 10 rods for $Opn1\ LW^{Tg};Rho^{REY/REY};Gcaps^{-/-}$). (*Right*) difference spectrum obtained by subtracting the spectrum of $Rho^{REY/REY};Gcaps^{-/-}$ rods from the spectrum of $Opn1\ LW^{Tg};Rho^{REY/REY};Gcaps^{-/-}$ rods was fitted by the waveform of single transducin response (red curve).

these spontaneous isomerization events has the same amplitude and kinetics as the corresponding responses to single absorbed photons because the molecules go through the same conformational changes (13). Hence, a steady thermal isomerization rate would be equivalent to a steady background light, leading to adaptation of the cell albeit in complete darkness. In the present study, we have recognized additionally that a dark continuous noise in native rod phototransduction, long observed by one of us (K-WY; see ref. 7), actually originates also from the visual pigment—although, for almost three decades, it has been reported (11; see also ref. 17) that this noise represents an intrinsic spontaneous activity of the PDE enzyme mediating phototransduction. We made this finding, partly unwittingly, upon replacing WT-Rho in rods with the "largely functionally silent" REY-Rho and noticing that this dark continuous noise disappeared, much against the expectation of no effect if it were associated with an intrinsic PDE activity, which is downstream of the pigment in transduction. This continuous noise comprises far more abundant unitary events despite their much smaller unitary amplitude than spontaneous isomerization, and appears to come from a metastable conformational state of the holopigment being intermittently active for very brief moments (see later).

Even more importantly, it now appears that a similar continuous noise is present in native cone holopigments as well. Previously, the presence of a continuous noise in native cones has been overlooked probably because the much smaller thermal isomerization events in native cones along with their somewhat similar kinetics as the continuous noise have rendered them difficult to be distinguished from each other (23, 24). In the experiments here, a comparison in the recordings between $Rho^{SW/REY};Gcaps^{-/-}$ rods and $Rho^{-/REY};Gcaps^{-/-}$ rods clearly showed a dark continuous noise associated with the presence of the Opn1-SW cone pigment (Fig. 7 *C* and *D*). The same was found when recordings from $Rho^{MW/REY};Gcaps^{-/-}$ rods and $Rho^{-/REY};Gcaps^{-/-}$ rods were compared, or recordings from $Opn1\text{-}LW^{Tg};Rho^{REY/REY};Gcaps^{-/-}$ rods and $Rho^{REY/REY};Gcaps^{-/-}$ rods (Fig. 7 *A*, *C*, *E*, and *F*). This noise was especially obvious when a

cone pigment was allowed to signal through the higher-gain rod phototransduction cascade, as done here, and in the *Gcaps*$^{-/-}$ genetic background to remove a major negative feedback. In addition, we ruled out the contribution of apo-opsin from cone pigments in this continuous noise. Our previous study showed that L-cone pigment, although not so much S- and M-cone pigments, tend to dissociate to some degree into apo-opsin and chromophore without isomerization in darkness (27). However, the contribution of apo-opsin to the dark noise of hOpn1-LW transgenic rods was not detected here (*SI Appendix*, Fig. S4) probably due to the very low expression level (~0.02%) of L-cone pigment in the transgenic rods.

Perhaps the greatest surprise is that the dark continuous noise from a cone holopigment is very substantial. This noise is much higher in magnitude than the corresponding isomerization (quantal) noise for a given cone pigment, and certainly much higher than the continuous noise in a native rod at a comparable rhodopsin expression level. When expressed in units of R* s^{-1} (equivalent background light), the continuous noise was ~895 R* s^{-1} for 100% mOpn1-SW, ~600 R* s^{-1} for 100% mOpn1-MW, and ~1,850 R* s^{-1} for 100% hOpn1-LW (*SI Appendix, Supplementary Text*), compared to only ~0.3 R* s^{-1} for 100% rhodopsin (all in the *Gcaps*$^{-/-}$ background). According to our previous estimate from native fish cones (27), up to 30% of Opn1-LW (although negligible for Opn1-SW and Opn1-MW pigments) is likely to dissociate into apo-opsin and chromophore, with the remainder as holopigment. At least for now, the dark continuous noise from cone apo-opsin versus from cone holopigment is not certain. For simplicity, we shall ignore here the contribution of the continuous noise from dissociated apo-opsin (although otherwise our argument would only be stronger). In any case, the equivalent background light from the remaining 70% hOpn1-LW holopigment would be ~1,850 × 0.7 = 1,295 R* s^{-1}. Now imagine a mouse rod with its entire rhodopsin content replaced by an equimolar amount of a cone pigment. Applying the equivalent background lights indicated above to such a rod obeying Weber's law, $S_F/S_F^D = I_O/(I_O + I_B)$ [where S_F is flash sensitivity in the presence of a background light I_B, S_F^D is flash sensitivity in the absence of background light (i.e., in darkness), and I_O is the background intensity that reduces the flash sensitivity in darkness by half (36)], the continuous noise produced by mOpn1-SW, mOpn1-MW, and hOpn1-LW would lead to an adaptation that reduces flash sensitivity by 25- to 50-fold (*SI Appendix*, Fig. S6). Thus, these adaptations would literally turn the rod more or less into a cone [cf. mouse rod flash sensitivity of ~0.18 pA photon^{-1} μm^2 (15) versus mouse cone sensitivity of ~0.003 pA photon^{-1} μm^2 (41)], giving a rod/cone sensitivity ratio of 60). As such, the dark continuous noise would by far be the most significant factor underlying the rod–cone difference in sensitivity in darkness (as well as the associated faster kinetics). On top of this, other factors such as the dissimilar rod/cone isoforms in phototransduction (rod/cone transducins, rod/cone PDEs, etc.) will also play some role. However, experiments by others mostly in mice, typically involving the substitution of a cone component for the corresponding rod component in rods (see ref. 42 for review), have suggested some reduction in sensitivity imposed by a cone isoform, but not always. These experiments nonetheless can sometimes be difficult to interpret because the interchange between rod/cone-isoforms usually involved just one particular subunit in a multimeric protein [e.g., rod PDE, which is a tetramer with one α, one β, and two γ subunits (43)], thus impossible to exclude unknown side-effects caused by nonnative subunit partners. Collectively, the general take-home message from these endeavors is that the correlation between protein isoforms and rod/cone response sensitivity and kinetics is somewhat diffuse and small (see ref. 42). Similarly small effects can be concluded regarding rod/cone differences in outer-segment volume and its intracellular disc geometry therein (44). Thus, except for the major contribution from the holopigment's dark continuous noise as found here, the downstream phototransduction components likely contribute only mildly to the response behavior. For the same reasons, expressing a cone pigment in tiny amounts (≤1% or less) in a rod environment, thus producing a minimal increase in the cone-pigment-associated dark continuous noise, is unlikely to render the cone-pigment signals much different from the rhodopsin signals, as indeed found (15, 16). If further verified, the dark continuous noise would be the most important factor underlying the sensitivity difference between rods and cones. Finally, any substantial continuous noise associated with cone pigment should also elevate the threshold of light detection in the host cones by reducing the signal-to-noise ratio (45).

What is the metastable pigment state? The interaction between (rod or cone) pigment and transducin is now known to involve the pigment's ERY motif at its third transmembrane domain near the cytoplasmic face (35, 46). This is most likely the region in rhodopsin and cone pigments (and many other G-protein-coupled receptors) that is exposed for interaction with G protein (transducin in this case). The power spectrum of the dark continuous noise in rods generated by this metastable state's activity is identical to that exhibited by apo-opsin (35), suggesting the similar brevity of these events and the transient exposure of the binding pocket. As found for the opsin-triggered dark continuous noise, the unitary electrical events are probably triggered by single $G_T\alpha^*$-PDE* complexes. The same continuous noise exists in a heavily exaggerated form in the disease-causing rhodopsin point mutant G90D, producing congenital stationary night blindness by causing a much higher frequency of these events in darkness (a continuous noise level ~1,000 fold higher than normal when expressed at the normal level in native rods) and making the host rod so adapted (47) as to be completely unable to signal dim light. Exactly the same noise is present in cone pigments under normal conditions but still higher in magnitude, ~2,000- to 6,000-fold higher than that in rods at the same expression level of rhodopsin and mostly explaining the very low sensitivity of cones. At present, it is unclear how this ERY region is exposed for interaction with transducin. Previously, it was found that the G90D mutation introduces an aspartic acid competing with E113 for forming the salt bridge with K296 (48). In WT-Rho, this salt bridge between E113 and K296 is a key constraint for maintaining the stability of the pigment (49), therefore an important regulator for the metastable conformational state. More biochemical and structural studies are necessary for uncovering the mystery of this metastable state.

Materials and Methods

All experiments were conducted according to the protocols approved by the Institutional Animal Care and Use Committee at Johns Hopkins University. The mouse Opn1-SW and Opn1-MW KI mouse lines were made at the transgenic core laboratory of Johns Hopkins University School of Medicine by using the CRISPR/Cas9 system. Suction-pipette recordings, analyses of flash responses and dark noise, power spectral analysis, and other experimental details are provided in *SI Appendix, Materials and Methods*.

Data, Materials, and Software Availability. All study data are included in the article and/or *SI Appendix*.

ACKNOWLEDGMENTS. We thank Drs. Jeannie Chen and Hui Xu at University of Southern California for sharing the *Gnat1*^{Tg} and *Gnat1*$^{-/-}$ mouse lines. We also thank Drs. Randall Reed and Jeremy Nathans at Johns Hopkins University for the kind help with the CRISPR design for *Rho*$^{SW/SW}$ and *Rho*$^{MW/MW}$ mouse lines, and all

members of the Yau laboratory for discussions. This work was supported by NIH Grants EY006837 (to K.-W.Y.), the António Champalimaud Vision Award, Portugal, the Helen Keller Prize, the Beckman-Argyros Award in Vision Research (to K.-W.Y.), and NS050274 (Multiphoton Imaging Core at Johns Hopkins University).

Author affiliations: [a]Solomon H. Snyder Department of Neuroscience, Johns Hopkins University School of Medicine, Baltimore, MD 21205; [b]Biochemistry, Cellular and Molecular Biology Graduate Program, Johns Hopkins University School of Medicine, Baltimore, MD 21205; and [c]Department of Ophthalmology, Johns Hopkins University School of Medicine, Baltimore, MD 21205

Author contributions: Z.C. and K.-W.Y. designed research; Z.C. performed research; Z.C., D.S., S.L., and P.B. contributed new reagents/analytic tools; Z.C., D.S., S.L., and K.-W.Y. analyzed data; and Z.C. and K.-W.Y. wrote the paper.

Reviewers: C.-K.J.C., University of Texas Health Science Center San Antonio; and T.G.W., Baylor College of Medicine.

The authors declare no competing interest.

1. M. E. Burns, V. Y. Arshavsky, Beyond counting photons: Trials and trends in vertebrate visual transduction. *Neuron* **48**, 387–401 (2005).
2. Y. Fu, K. W. Yau, Phototransduction in mouse rods and cones. *Pflugers Arch.* **454**, 805–819 (2007).
3. D. G. Luo, T. Xue, K. W. Yau, How vision begins: An odyssey. *Proc. Natl. Acad. Sci. U.S.A.* **105**, 9855–9862 (2008).
4. F. A. Dodge Jr., B. W. Knight, J. Toyoda, Voltage noise in Limulus visual cells. *Science* **160**, 88–90 (1968).
5. T. D. Lamb, E. J. Simon, Analysis of electrical noise in turtle cones. *J. Physiol.* **272**, 435–468 (1977).
6. K. W. Yau, G. Matthews, D. A. Baylor, Thermal activation of the visual transduction mechanism in retinal rods. *Nature* **279**, 806–807 (1979).
7. D. A. Baylor, G. Matthews, K. W. Yau, Two components of electrical dark noise in toad retinal rod outer segments. *J. Physiol.* **309**, 591–621 (1980).
8. D. A. Baylor, B. J. Nunn, J. L. Schnapf, The photocurrent, noise and spectral sensitivity of rods of the monkey Macaca fascicularis. *J. Physiol.* **357**, 575–607 (1984).
9. J. L. Schnapf, B. J. Nunn, M. Meister, D. A. Baylor, Visual transduction in cones of the monkey Macaca fascicularis. *J. Physiol.* **427**, 681–713 (1990).
10. D. M. Schneeweis, J. L. Schnapf, Noise and light adaptation in rods of the macaque monkey. *Vis. Neurosci.* **17**, 659–666 (2000).
11. F. Rieke, D. A. Baylor, Molecular origin of continuous dark noise in rod photoreceptors. *Biophys. J.* **71**, 2553–2572 (1996).
12. G. J. Jones, Membrane current noise in dark-adapted and light-adapted isolated retinal rods of the larval tiger salamander. *J. Physiol.* **511**, 903–913 (1998).
13. D. G. Luo, W. W. Yue, P. Ala-Laurila, K. W. Yau, Activation of visual pigments by light and heat. *Science* **332**, 1307–1312 (2011).
14. K. Donner, M. L. Firsov, V. I. Govardovskii, The frequency of isomerization-like "dark" events in rhodopsin and porphyropsin rods of the bull-frog retina. *J. Physiol.* **428**, 673–692 (1990).
15. Y. Fu, V. Kefalov, D. G. Luo, T. Xue, K. W. Yau, Quantal noise from human red cone pigment. *Nat. Neurosci.* **11**, 565–571 (2008).
16. V. Kefalov, Y. Fu, N. Marsh-Armstrong, K. W. Yau, Role of visual pigment properties in rod and cone phototransduction. *Nature* **425**, 526–531 (2003).
17. U. Bocchero, J. Pahlberg, Origin of discrete and continuous dark noise in rod photoreceptors. *eNeuro* **10**, ENEURO.0390-23.2023 (2023).
18. S. Hecht, S. Shlaer, M. H. Pirenne, Energy, quanta, and vision. *J. Gen. Physiol.* **25**, 819–840 (1942).
19. K. Donner, Noise and the absolute thresholds of cone and rod vision. *Vision Res.* **32**, 853–866 (1992).
20. J. Nathan *et al.*, Scotopic and photopic visual thresholds and spatial and temporal discrimination evaluated by behavior of mice in a water maze. *Photochem. Photobiol.* **82**, 1489–1494 (2006).
21. Y. Umino, E. Solessio, R. B. Barlow, Speed, spatial, and temporal tuning of rod and cone vision in mouse. *J. Neurosci.* **28**, 189–198 (2008).
22. F. Naarendorp *et al.*, Dark light, rod saturation, and the absolute and incremental sensitivity of mouse cone vision. *J. Neurosci.* **30**, 12495–12507 (2010).
23. F. Rieke, D. A. Baylor, Origin and functional impact of dark noise in retinal cones. *Neuron* **26**, 181–186 (2000).
24. A. P. Sampath, D. A. Baylor, Molecular mechanism of spontaneous pigment activation in retinal cones. *Biophys. J.* **83**, 184–193 (2002).
25. V. J. Kefalov *et al.*, Breaking the covalent bond–a pigment property that contributes to desensitization in cones. *Neuron* **46**, 879–890 (2005).
26. D. Holcman, J. I. Korenbrot, The limit of photoreceptor sensitivity: Molecular mechanisms of dark noise in retinal cones. *J. Gen. Physiol.* **125**, 641–660 (2005).
27. D. G. Luo *et al.*, Apo-opsin and its dark constitutive activity across retinal cone subtypes. *Curr. Biol.* **30**, 4921–4931.e5 (2020).
28. D. M. Schneeweis, J. L. Schnapf, The photovoltage of macaque cone photoreceptors: Adaptation, noise, and kinetics. *J. Neurosci.* **19**, 1203–1216 (1999).
29. J. M. Angueyra, F. Rieke, Origin and effect of phototransduction noise in primate cone photoreceptors. *Nat. Neurosci.* **16**, 1692–1700 (2013).
30. J. Baudin, J. M. Angueyra, R. Sinha, F. Rieke, S-cone photoreceptors in the primate retina are functionally distinct from L and M cones. *Elife* **8**, e39166 (2019).
31. D. A. Baylor, T. D. Lamb, K. W. Yau, The membrane current of single rod outer segments. *J. Physiol.* **288**, 589–611 (1979).
32. D. A. Baylor, T. D. Lamb, K. W. Yau, Responses of retinal rods to single photons. *J. Physiol.* **288**, 613–634 (1979).
33. W. W. S. Yue *et al.*, Spontaneous activation of visual pigments in relation to openness/closedness of chromophore-binding pocket. *Elife* **6**, e18492 (2017).
34. A. Mendez *et al.*, Role of guanylate cyclase-activating proteins (GCAPs) in setting the flash sensitivity of rod photoreceptors. *Proc. Natl. Acad. Sci. U.S.A.* **98**, 9948–9953 (2001).
35. W. W. S. Yue *et al.*, Elementary response triggered by transducin in retinal rods. *Proc. Natl. Acad. Sci. U.S.A.* **116**, 5144–5153 (2019).
36. D. Silverman *et al.*, Dark noise and retinal degeneration from D190N-rhodopsin. *Proc. Natl. Acad. Sci. U.S.A.* **117**, 23033–23043 (2020).
37. W. He, C. W. Cowan, T. G. Wensel, RGS9, a GTPase accelerator for phototransduction. *Neuron* **20**, 95–102 (1998).
38. C. K. Chen *et al.*, Slowed recovery of rod photoresponse in mice lacking the GTPase accelerating protein RGS9-1. *Nature* **403**, 557–560 (2000).
39. C. M. Krispel *et al.*, RGS expression rate-limits recovery of rod photoresponses. *Neuron* **51**, 409–416 (2006).
40. B. Katz, R. Miledi, The statistical nature of the acetylcholine potential and its molecular components. *J. Physiol.* **224**, 665–699 (1972).
41. L. H. Cao, D. G. Luo, K. W. Yau, Light responses of primate and other mammalian cones. *Proc. Natl. Acad. Sci. U.S.A.* **111**, 2752–2757 (2014).
42. N. T. Ingram, A. P. Sampath, G. L. Fain, Why are rods more sensitive than cones? *J. Physiol.* **594**, 5415–5426 (2016).
43. N. O. Artemyev, R. Surendran, J. C. Lee, H. E. Hamm, Subunit structure of rod cGMP-phosphodiesterase. *J. Biol. Chem.* **271**, 25382–25388 (1996).
44. A. Morshedian, G. L. Fain, Single-photon sensitivity of lamprey rods with cone-like outer segments. *Curr. Biol.* **25**, 484–487 (2015).
45. L. Smeds *et al.*, Paradoxical rules of spike train decoding revealed at the sensitivity limit of vision. *Neuron* **104**, 576–587.e11 (2019).
46. R. R. Franke, B. König, T. P. Sakmar, H. G. Khorana, K. P. Hofmann, Rhodopsin mutants that bind but fail to activate transducin. *Science* **250**, 123–125 (1990).
47. Z. Chai *et al.*, Dark continuous noise from mutant G90D-rhodopsin predominantly underlies congenital stationary night blindness. *Proc. Natl. Acad. Sci. U.S.A.* **121**, e2404763121 (2024).
48. A. Singhal *et al.*, Insights into congenital stationary night blindness based on the structure of G90D rhodopsin. *EMBO Rep.* **14**, 520–526 (2013).
49. J. M. Kim *et al.*, Structural origins of constitutive activation in rhodopsin: Role of the K296/E113 salt bridge. *Proc. Natl. Acad. Sci. U.S.A.* **101**, 12508–12513 (2004).